Journal of Materials Chemistry A

Achieving High Room-Temperature Thermoelectric Performance in Cubic AgCuTe

Journal:	*Journal of Materials Chemistry A*
Manuscript ID	TA-ART-11-2019-012954.R1
Article Type:	Paper
Date Submitted by the Author:	27-Jan-2020
Complete List of Authors:	Jiang, Jing; University of Electronic Science and Technology of China; University of Houston Zhu, Hangtian; University of Houston Niu, Yi; University of Electronic Science and Technology of China Zhu, Qing; University of Houston Song, Shaowei ; University of Houston Zhou, Ting; University of Electronic Science and Technology of China; University of Houston Wang, Chao; University of Electronic Science and Technology of China Ren, Zhifeng; University of Houston

Achieving High Room-Temperature Thermoelectric Performance in Cubic AgCuTe

Jing Jiang[1, 2, #], Hangtian Zhu[2, #], Yi Niu[1, #], Qing Zhu[2], Shaowei Song[2], Ting Zhou[1, 2], Chao Wang[1, *], Zhifeng Ren[2, *]

[1]Clean Energy Materials and Engineering Center, State Key Laboratory of Electronic Thin Film and Integrated Device, School of Electronic Science and Engineering, University of Electronic Science and Technology of China, Chengdu 611731, China

[2]Department of Physics and TcSUH, University of Houston, Houston, Texas 77204, USA

[*]E-mail: cwang@uestc.edu.cn; zren@uh.edu

[#]These authors contributed equally to this work

Although there has been significant progress in developing high-temperature thermoelectric materials, seeking promising near-room-temperature candidates has been extremely difficult, and the discovery of such materials, which would be beneficial for low-grade waste-heat power generation and cooling near room temperature, has been rarely reported. Here we report the enhanced near-room-temperature performance (ZT_{max} = ~1.1 at 350 K, ZT_{avg} = ~1.0 between 300 K and 673 K) of copper chalcogenide $(AgCu)_{0.995}Te_{0.9}Se_{0.1}$ by successfully stabilizing the face-centered cubic (FCC) phase at room temperature. Surprisingly low lattice thermal conductivity (~0.4 W m^{-1} K^{-1}) and a good power factor (~13.8 μW cm^{-1} K^{-2}) are simultaneously achieved near room temperature due to the unique properties of the FCC phase. A competitive conversion efficiency of 11% is obtained in a $(AgCu)_{0.995}Te_{0.9}Se_{0.1}$–based single leg at a low temperature difference of 400 K. The high thermal stability and low operating temperature, combined with the economically competitive efficiency, will greatly promote the application of $(AgCu)_{0.995}Te_{0.9}Se_{0.1}$-based devices in power generation from low- and medium-grade waste heat. The results also indicate a new strategy to improve the near-room-temperature performance and stability of copper chalcogenide thermoelectric materials and a new direction for further research.

Introduction

Due to their small size and their lack of noise, vibration, and gas emission, thermoelectric devices are one of the most popular solid-state energy converters for near-room-temperature cooling and power generation. These devices are highly competitive in applications of miniature cooling systems such as in car seats, night-vision systems, integrated circuits, and even miniature refrigerators [1], and are also irreplaceable for low-grade (below 473K) waste-heat power generation, e.g., in the smart home and Internet of Things (IoT). All of these applications require near-room-temperature high-performance thermoelectric devices. However, compared to their counterparts used in high temperature, it is relatively difficult to develop high-efficiency thermoelectric devices for room-temperature application due to the small temperature difference and limitation of Carnot efficiency:

$$\eta = \left(\frac{T_{\mathrm{H}} - T_C}{T_{\mathrm{H}}} \right) \left[\frac{\sqrt{1+ZT_{\mathrm{avg}}} - 1}{\sqrt{1+ZT_{\mathrm{avg}}} + \left(\frac{T_{\mathrm{C}}}{T_H} \right)} \right] \quad (1)$$

where T_{H} and T_{C} are the hot-side and cold-side temperatures of the device, respectively, and ZT_{avg} is the average ZT value.

Therefore, for room-temperature applications, the only effective approach to promote the energy conversion efficiency of thermoelectric devices is to improve the Z value of material, which is determined by the intrinsic transport properties of thermoelectric material: $Z = S^2\sigma/(\kappa_{\mathrm{e}}+\kappa_{\mathrm{L}})$, where S, σ, κ_{e}, and κ_{L} are the Seebeck coefficient, electrical conductivity, electronic thermal conductivity, and lattice thermal conductivity, respectively. High Z requires a large Seebeck coefficient (S), high electrical conductivity (σ), and poor thermal conductivity ($\kappa = \kappa_{\mathrm{e}}+\kappa_{\mathrm{L}}$). However, the strong conflicting correlations among S, σ, and κ_{e} make it difficult to simultaneously improve all the parameters to obtain a high Z value. In recent years, new strategies to decouple the contradicting transport properties have been developed, such as band structure engineering [2-5], multi-scale phonon scattering [6-12], the

introduction of resonant levels [13-18], etc., which have proven successful in improving thermoelectric properties of various materials. Due to the relentless effort applied to these approaches, the record for peak *ZT* has been unceasingly broken, increasing from 1 to 2.8 for a wide range of thermoelectric materials, including PbTe [13, 19], Zintls [20-23], $AgPb_mSbTe_{m+2}$ [24], skutterudites [25-27], clathrates [28, 29], SnSe single crystals [30], copper chalcogenides [31-36], SiGe [37], and half-Heusler alloys [38-40], etc. However, most of above achievements focus on the peak *ZT* at high temperature (600-1000 K) benefiting from the higher *T* value and lower lattice thermal conductivity due to the strong Umklapp scattering at high temperature, and all of the current state-of-the-art thermoelectric materials, except for Bi_2Te_3 [12, 41-43] and MgAgSb [44], exhibit poor *ZT*s at low, especially near-room temperatures. Therefore, improving the low-temperature performance is a challenge and crucial for thermoelectric material, because the application at room temperature is its core competitiveness.

An alternative way to achieve high low-temperature *ZT*s is searching for new materials with intrinsically low κ_L and unique band structures [45-48]. As one of the best thermoelectric materials, superionic phases of copper chalcogenides Cu_2X or AgCuX (X= S, Se, or Te), possess a cubic structure with high mobility [49] and an extraordinarily low κ_L, even below that of a glass [31]. Their unique liquid-like behavior provides a strong phonon scattering and the reduces specific heat *C*v by suppressing of transverse phonon modes [32]. The distinctive approach for κ_L suppression, as well as the high thermoelectric performance in superionic copper chalcogenides, point out a new direction for developing novel room-temperature candidates. Nevertheless, cubic copper chalcogenides are likely to exist only at higher temperatures. With decreasing temperature, copper chalcogenides undergo one or more phase transitions from the cubic structure to non-cubic structures [34, 48, 50-53], such as the orthorhombic structure of AgCuSe and the chalcocite structure of Cu_2S, in which Cu/Ag atoms are localized and κ_L is much higher. Studies have shown that the phase relation of copper chalcogenides at low-temperature phases is strongly

affected by their non-stoichiometric compositions, which are complicated and are not yet fully understood [54]. The low-temperature phases of Cu_2Se, for example, have been reported by different groups to be monoclinic, tetragonal, orthorhombic, or a mixture of several phases [31, 55, 56]. A few studies have also shown that the high-temperature cubic structure of Cu_2Se could be partially retained at room temperature upon a considerable deficiency of copper atoms [54]. However, achieving a relatively pure cubic phase at room temperature is extremely challenging, not to mention to control the carrier concentration and realize an outstanding thermoelectric performance. In this work, we report the synthesis and investigation of the room-temperature cubic phase of copper chalcogenide $(AgCu)_{1-x}Te_{0.9}Se_{0.1}$, which displays promising thermoelectric properties in a wide temperature range from room temperature to 673 K.

Results

With the simultaneous increase in power factor ($PF = S^2\sigma$) and decrease in thermal conductivity, a maximum ZT of ~1.1 at 350 K and an average ZT, $(ZT)_{avg}$, of near unity between 300 K and 673 K were obtained for Se alloyed $(AgCu)_{0.995}Te_{0.9}Se_{0.1}$, as shown in Fig. 1. The enhanced performance is attributed to the successful stabilization of the face-centered cubic (FCC) phase at room temperature by Se alloying. As compared with a complex non-cubic phase of AgCuTe, the room-temperature ZT is enhanced by 10-20 times for the FCC phase of $AgCuTe_{0.9}Se_{0.1}$ (see Fig. S1, Supporting Information). The superior performance is demonstrated in Fig. 1 as compared with recently reported important p-type materials and other copper chalcogenides with non-room-temperature-cubic structures. The best low-temperature performance in non-room-temperature-cubic copper chalcogenides to date was recently reported by J.-Y. Tak *et al*., who achieved a maximum ZT of ~0.9 at 390 K and an average ZT of ~0.7 between room temperature and 390 K in monoclinic $Cu_{2.075}Se$ [48]. This is a significant improvement, but its performance seriously deteriorates above 390 K [Fig. 1(a)] due to the phase transition. Other reported copper chalcogenides show obviously lower ZT values around room

temperature, and most of *ZT* values are less than 0.4 even when the temperature increases to near 500 K [Fig. 1(a)]. Additionally, the $(ZT)_{avg}$ between 300 K and 673 K in this work is doubled compared with other reported copper chalcogenides and most p-type materials [Fig. 1(b)]. A theoretical high conversion efficiency of ~12% was calculated under such an enhanced $(ZT)_{avg}$, indicating that the copper chalcogenides could be a potential substitute for Bi_2Te_3, especially for filling the *ZT* gap left by Bi_2Te_3 at higher temperatures.

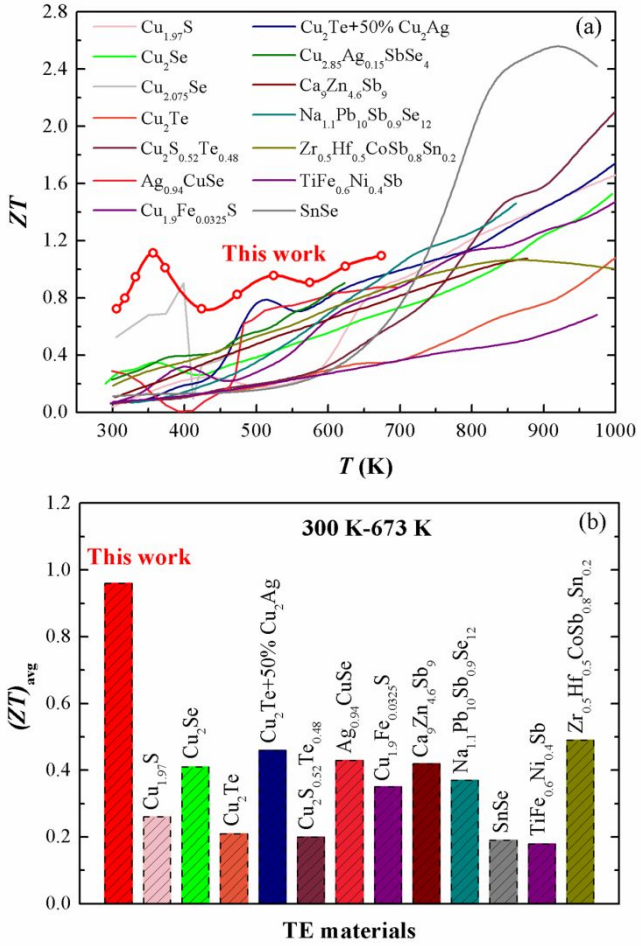

Fig. 1. Enhanced near-room-temperature and middle-temperature *ZT* values in $(AgCu)_{0.995}Te_{0.9}Se_{0.1}$ (this work). (a) Temperature dependence of *ZT* values of $(AgCu)_{0.995}Te_{0.9}Se_{0.1}$ and other p-type materials from previously reported studies ($Cu_{1.97}S$ [32], Cu_2Se [31], $Cu_{2.075}Se$ [48], Cu_2Te [57], $Cu_2S_{0.52}Te_{0.48}$ [33], $Ag_{0.94}CuSe$ [50], $Cu_{1.9}Fe_{0.0325}S$ [58], Cu_2Te+50% Cu_2Ag [59], $Cu_{2.85}Ag_{0.15}SbSe_4$ [60], $Ca_9Zn_{4.6}Sb_9$ [23], $Na_{1.1}Pb_{10}Sb_{0.9}Se_{12}$ [61], $Zr_{0.5}Hf_{0.5}CoSb_{0.8}Sn_{0.2}$ [62], $TiFe_{0.6}Ni_{0.4}Sb$ [63], and SnSe [30]). (b) Average *ZT* values $[(ZT)_{avg}]$ between 300 K and 673 K for $(AgCu)_{0.995}Te_{0.9}Se_{0.1}$ and other p-type materials calculated by the formula of $(ZT)_{avg} = Z_{int}T_{avg}$, where $Z_{int} = \frac{1}{T_h - T_c}\int_{T_c}^{T_h} Z(T)dT$ and $T_{avg} = \frac{T_h + T_c}{2}$ [64].

The room-temperature cubic phase was obtained by Se alloying and confirmed

by the room-temperature X-ray diffraction (XRD) patterns as shown in Fig. 2(a). As-prepared AgCuTe exhibits a complex phase relation at room temperature, but with 10% Se alloying, the diffraction peaks of the main phase can be indexed as a face-centered cubic (FCC) structure with a lattice constant of 6.216 Å. The inset of Fig. 2(a) shows the possible cubic crystal structure of $AgCuTe_{0.9}Se_{0.1}$, where Te/Se atoms compose the regular FCC framework, while Cu^+/Ag^+ ions occupy the interstitial positions (the green octahedral and the dark yellow tetrahedral sites).

Considering the thermal expansion of material, there will generally be a gradual diminution of interstitial space as temperature decreases, making the high-temperature FCC phase increasingly unstable until it finally transforms into a stable low-symmetry phase at low-temperature. Therefore, we replaced a portion of the Te atoms with Se atoms of smaller size to increase the interstitial space and stabilize the FCC phase of $AgCuTe_{0.9}Se_{0.1}$ at low temperature. As shown in the XRD pattern [Fig. 2(a)], a small amount of impurity phases remained with the main FCC phase, and no improvement could be obtained by adjustment of the Se content or the Ag/Cu ratio. Actually, increasing the Se content to more than 20% or changing the Ag/Cu ratio far away from 1:1 significantly increases the concentration of impurity phases (see Figs. S2 and S3, Supporting Information). The fixed Ag/Cu ratio may be due to the fixed Ag atom in the octahedral sites of the low temperature phase. The Cu atom may locate in half of the tetrahedral sites (half-Heusler structure) or randomly distribute and move among all the tetrahedral sites. More carefully investigation and calculation are required in the future to understand this FCC structure. However, as shown in the temperature-dependent XRD analyses (see Fig. S4, Supporting Information), the impurity phases begin to dissolve into the main FCC phase with increasing temperature over 423 K, and no obvious impurity can be observed when temperature is as high as 623 K. The actual mechanism for the formation of the room-temperature FCC phase remains unclear and further study is needed.

The room-temperature high-resolution transmission electron microscopy (HRTEM) analysis of $AgCuTe_{0.9}Se_{0.1}$ further confirms the FCC structure, as shown in

Fig. 2(b) and Fig. S5 (Supporting Information). The lattice constant was measured to be 6.2 Å, consistent with the XRD result. The EDS analysis indicates that the composition of the FCC phase is close to $AgCuTe_{0.9}Se_{0.1}$ (see Fig. S6, Supporting Information). Moreover, the FCC phase has proven to be very stable during thermal treatment. It was almost completely unchanged after a series of thermoelectric properties measurements at temperatures up to 673 K and even after a 4-month annealing treatment at about 360 K in air (see Fig. S7, Supporting Information).

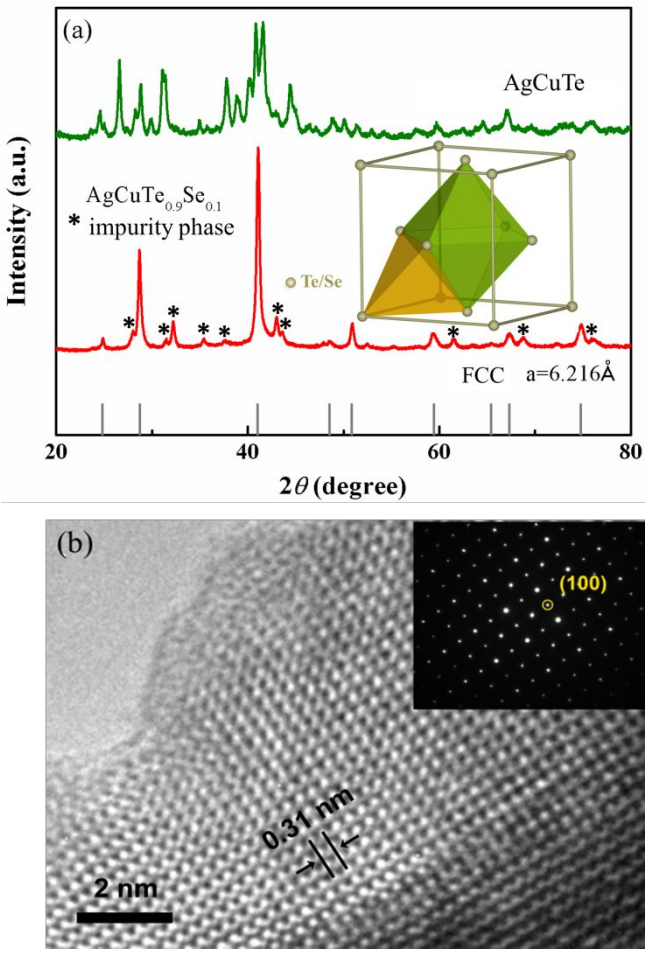

Fig. 2. Room-temperature XRD and HRTEM analyses of $AgCuTe_{0.9}Se_{0.1}$. (a) XRD patterns of the as-prepared AgCuTe and $AgCuTe_{0.9}Se_{0.1}$ samples at room temperature. Inset: unit cell of $AgCuTe_{0.9}Se_{0.1}$, in which Cu^{+}/Ag^{+} ions locate in two interstitial sites, the green octahedral and the dark yellow tetrahedral. (b) HRTEM image and its fast Fourier transform (FFT) diffractogram of the $AgCuTe_{0.9}Se_{0.1}$ sample at room temperature. The spacing of 0.31 nm corresponds to (200), indicating that the lattice constant is 0.62 nm (6.2 Å).

The comparisons of thermoelectric properties between AgCuTe and $AgCuTe_{0.9}Se_{0.1}$ are shown in Fig. S1 (Supporting Information). Due to the main cubic phase of the Se alloyed sample, the electronic properties are significantly improved.

The electrical behavior transforms from metal to semiconductor, which is much more favorable for thermoelectrics. Consequently, the power factor increases by ~500% and *ZT* is thus enhanced by 10-20 times for the FCC phase of $AgCuTe_{0.9}Se_{0.1}$. Moreover, as the temperature increase, all the transport properties of AgCuTe fluctuate at ~450 K, including electrical conductivity, Seebeck coefficient, and thermal conductivity, which should be attributed to the dissolution process of the impurity phases (Fig. S4).

The carrier concentration of $AgCuTe_{0.9}Se_{0.1}$ was further optimized by slightly adjusting the vacancy of Ag/Cu. Table S1 (Supporting Information) shows the room-temperature Hall carrier concentrations for the $(AgCu)_{1-x}Te_{0.9}Se_{0.1}$ (x=-0.025, 0, 0.005, 0.01, 0.075) samples. Fig. 3 shows the temperature dependence of thermoelectric properties. Due to the intrinsic Ag/Cu deficiency, even in the sample with excess Ag/Cu content, holes remain as the dominant charge carriers. Additional Ag/Cu vacancy was introduced to adjust the carrier concentration and to optimize the power factor. As shown in Fig. 3(a) and 3(b), with increasing Ag/Cu vacancy from $AgCuTe_{0.9}Se_{0.1}$ to $(AgCu)_{0.925}Te_{0.9}Se_{0.1}$, the electrical conductivity (σ) increases, leading to a reduced Seebeck coefficient (S). The electronic properties follow this trend very well at a high temperature where only peaks of the FCC phase can be observed in the XRD pattern (see Fig. S4, Supporting Information). However, at low temperatures, the impurity is vacancy concentration-dependent, and thus the trend is more complicated. The $(AgCu)_{0.995}Te_{0.9}Se_{0.1}$ possesses the highest S but not the lowest σ, which may due to the competition between the main FCC phase and impurity phases on electronic transport. Both the S and σ increase with the rising temperature [Fig. 3(a) and 3(b)], and a peak power factor of about 13.8 $\mu W\ cm^{-1}\ K^{-2}$ was obtained in $(AgCu)_{0.995}Te_{0.9}Se_{0.1}$ at about 350 K, which is twice as high as that of $AgCuTe_{0.9}Se_{0.1}$ [Fig. 3(c)]. The dissolution process of the impurity phase with rising temperature (Fig. S4) may be the reason for the deterioration of electronic transport properties above 350 K. The power factor would possibly be further improved if a pure room-temperature FCC phase could be achieved.

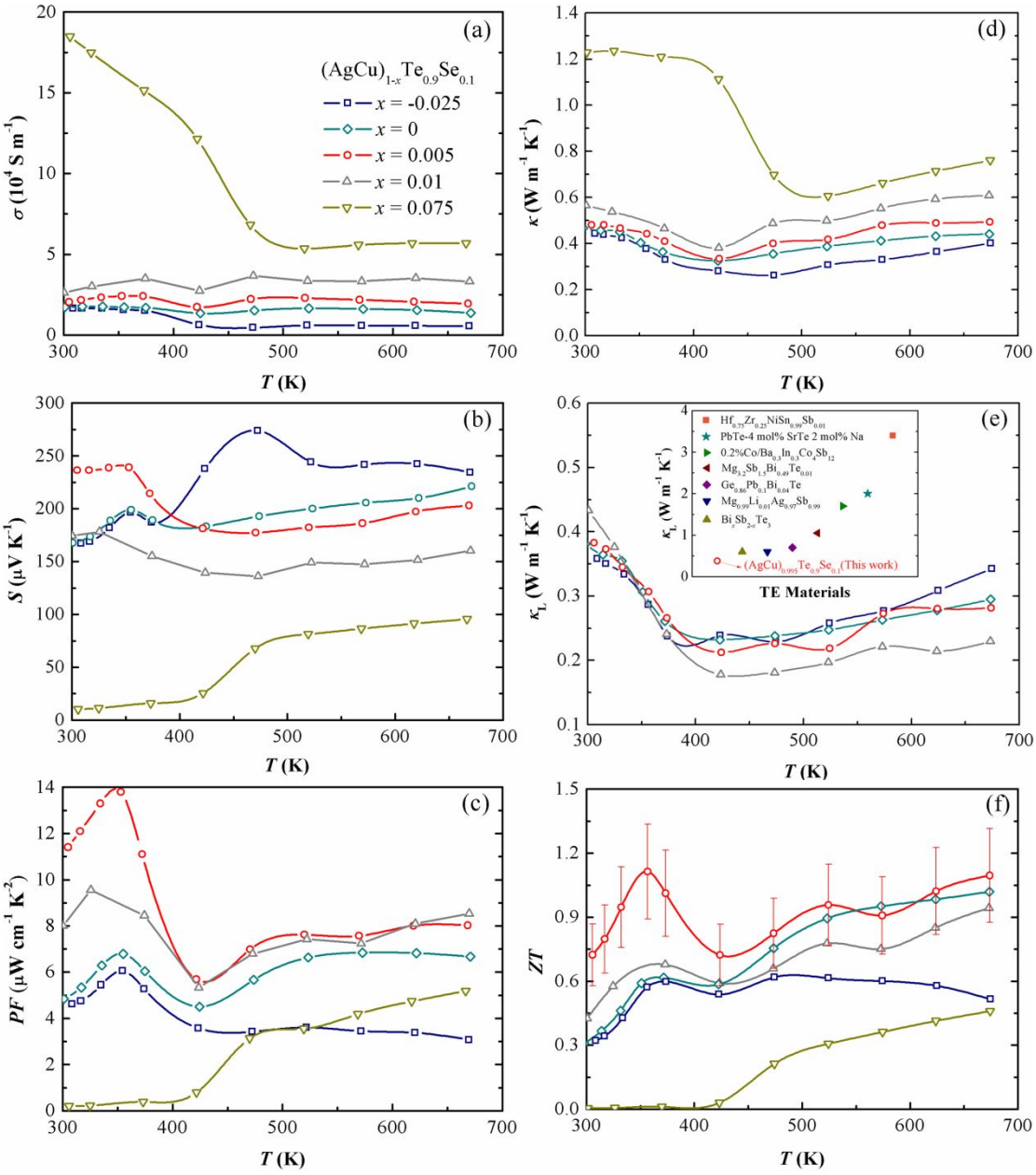

Fig. 3. Temperature dependence of thermoelectric properties for $(AgCu)_{1-x}Te_{0.9}Se_{0.1}$ (x = -0.025, 0, 0.005, 0.01, and 0.075) samples. (a) Electrical conductivity (σ). (b) Seebeck coefficient (S). (c) Power factor (PF). (d) Total thermal conductivity (κ). (e) Lattice thermal conductivity (κ_L). Inset: κ_L of $(AgCu)_{0.995}Te_{0.9}Se_{0.1}$ and other state-of-the-art thermoelectric materials at room temperature ($Bi_xSb_{2-x}Te_3$ [12], $Mg_{0.99}Li_{0.01}Ag_{0.97}Sb_{0.99}$ [45], $Ge_{0.86}Pb_{0.1}Bi_{0.04}Te$ [65], $Mg_{3.2}Sb_{1.5}Bi_{0.49}Te_{0.01}$ [22], $0.2\%Co/Ba_{0.3}In_{0.3}Co_4Sb_{12}$ [66], PbTe-4 mol% SrTe 2 mol% Na [19], and $Hf_{0.75}Zr_{0.25}NiSn_{0.99}Sb_{0.01}$ [67]). (f) ZT values. The uncertainty for ZT is about 20%.

Fig. 3(d) shows the temperature dependence of the total thermal conductivity (κ). $(AgCu)_{0.925}Te_{0.9}Se_{0.1}$ exhibits a relatively high thermal conductivity (~1.2 W m^{-1} K^{-1}) at near-room temperatures due to the impurity and the large electrical conductivity at low temperature. The other samples possess relatively low thermal conductivities (below 0.6 W m^{-1} K^{-1}) over the whole temperature range from 300 K to 673 K. The

calculated lattice thermal conductivities (κ_L) are around 0.35-0.45 W m^{-1} K^{-1} at room temperature for all of the samples [Fig. 3(e)]. It is difficult to realize such very low κ_L in a fully densified solid at room temperature. Clearly, the room-temperature κ_L of $(AgCu)_{0.995}Te_{0.9}Se_{0.1}$ is much lower than most of other state-of-the-art thermoelectric materials [inset, Fig. 3(e)]. At higher temperatures, as all impurities disappear, κ_L decreases with increasing Ag/Cu vacancy due to stronger phonon scattering by the point defects, falling to ~0.2-0.3 W m^{-1} K^{-1}, almost one of the lowest room temperature κ_L values ever achieved among state-of-the-art thermoelectric materials [68, 69].

The samples are highly dense with densities varying from 7.93 to 8.04 g cm^{-3} except for $(AgCu)_{0.925}Te_{0.9}Se_{0.1}$, which has a density of only 6.95 g cm^{-3} due to large amounts of impurities (see Table S1, Supporting Information). Assuming that all atoms completely occupy the sites in the cubic structure, the upper limit of the theoretical density can be estimated to be 8.11 g cm^{-3}. Therefore, the relative density for the $(AgCu)_{1-x}Te_{0.9}Se_{0.1}$ (x=-0.025, 0, 0.005, 0.01) samples is above 97%, indicating the samples are highly dense. It should be noted that all of the samples were hot-pressed at a low temperature of only 473 K. The high mobility of the Cu^+/Ag^+ ions enables the production of a well-distributed and well-sintered sample at such a low temperature (see Figs. S8 and S9, Supporting Information). It is worth mentioning that the high hot-press temperature of 923 K results in a large number of highly oriented cracks in the samples, likely caused by the volatilization of Se and Te (see Fig. S10, Supporting Information). The oriented cracks may lead to highly anisotropic properties even for the materials with cubic structure as we observed in some cases of hot pressed half-Heuslers, and a much higher invalid ZT may be obtained by the combination of the thermal conductivity measured parallel to the hot-press direction and the electronic properties measured perpendicular to the hot-press direction (see Fig. S11, Supporting Information). The cracks remain but become smaller and more weakly oriented when the hot-press temperature decreases to 823 K (see Fig. S12, Supporting Information). By further reducing the hot-press

temperature, the anisotropy finally vanishes with the disappearance of cracks, as shown in the cross-sectional scanning electron microscopy (SEM) image of the sample hot-pressed at 473 K (Fig. S8), and highly dense samples are obtained. The isotropic thermal conductivity values along different directions were further confirmed by the efficiency measurement.

The *ZT* values are shown in Fig. 3f. Combined with the optimized power factor and low thermal conductivities, $(AgCu)_{0.995}Te_{0.9}Se_{0.1}$ demonstrates very good performance over the entire temperature range studied in this work. Its low-temperature *ZT*s are almost twice the value of $AgCuTe_{0.9}Se_{0.1}$, and the peak value of ~1.1 is obtained at 350 K. However, the performance deteriorates seriously with excessive Ag/Cu deficiencies which could not be used to stable the cubic phase in this material system. With Ag/Cu vacancy increasing to 7.5%, the sample exhibits near-zero room-temperature *ZT*s due to a large amount of impurity phases (see Fig. S13, Supporting Information).

To verify the reliability and to appraise the thermal stability of $(AgCu)_{0.995}Te_{0.9}Se_{0.1}$, the sample was first measured six times from 300 K to 373 K and then measured again from 300 K to 673 K six times. The results of repeated measurement at low-temperature (300 K-373 K) are shown in Fig. S14 (Supporting Information). The relative variations in all thermoelectric properties are no more than 5% within the six measurements. Among the repeated high-temperature measurements (300 K to 673 K), the largest relative variations in electrical conductivity and Seebeck coefficient are no more than 10% (see Fig. S15, Supporting Information). The power factor and the thermal conductivity are almost the same over six high-temperature measurements [Fig. 4(a)-(c)], confirming high reliability and indicating the good thermal stability of the sample with temperatures up to 673 K.

Additionally, the reproducibility of thermoelectric properties of $(AgCu)_{0.995}Te_{0.9}Se_{0.1}$ was studied with four samples of different batches, as shown in Fig. 4(d)-(f). The relative differences in the electrical conductivity and Seebeck coefficient are comparable (see Fig. S16, Supporting Information), and the difference

in power factor is no more than 10% over the whole temperature range measured in this work. The thermal conductivities are similar over the entire temperature range, except that of the third sample at temperatures above 550 K, which may be caused by unknown measurement errors. As a result, the largest variation in *ZT* is below 13% throughout the studied temperature range, indicating the good reproducibility of this material.

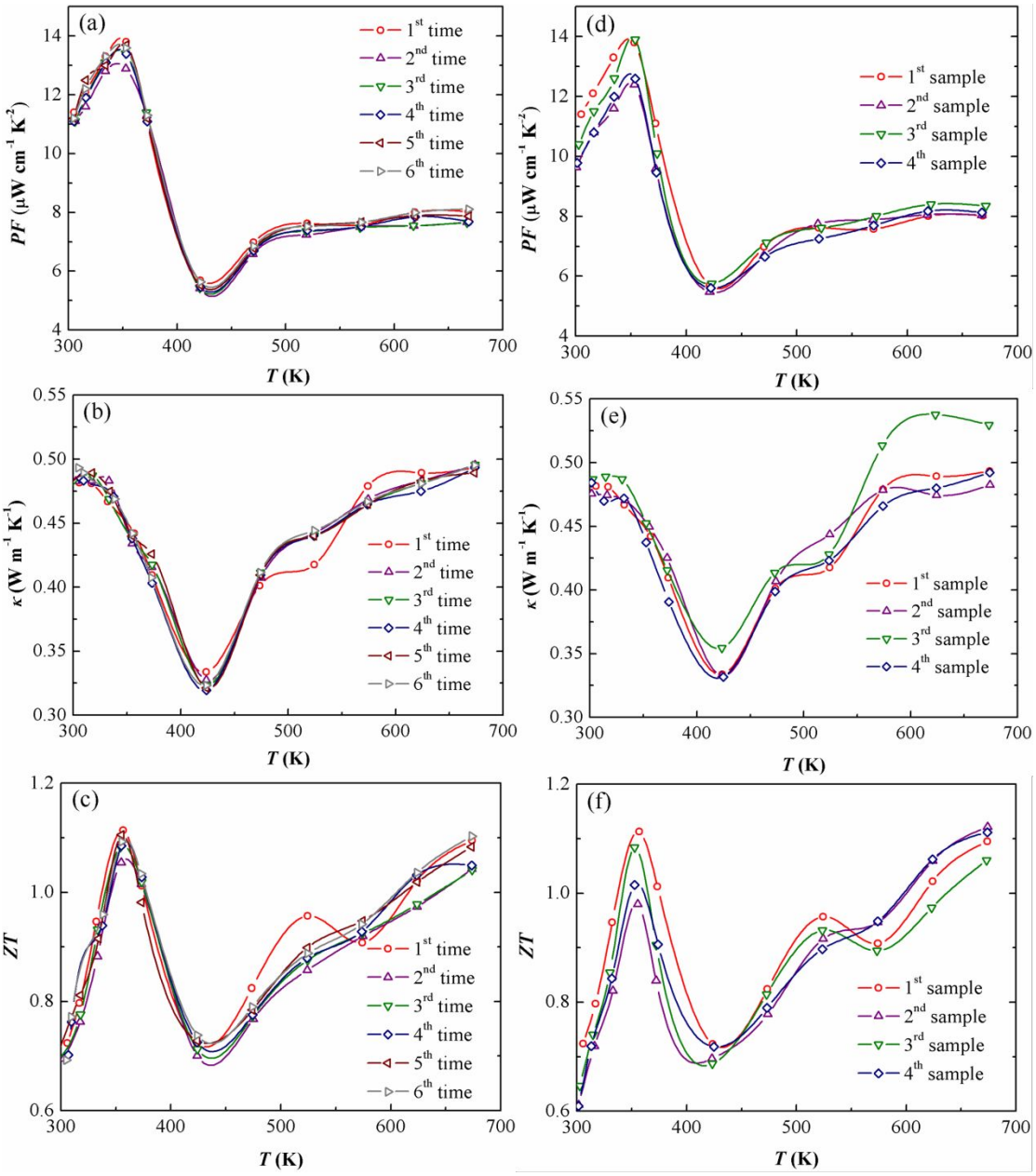

Fig. 4. High stability and reproducibility of thermoelectric properties of $(AgCu)_{0.995}Te_{0.9}Se_{0.1}$. Temperature dependence of (a) power factor (*PF*), (b) thermal conductivity (κ), and (c) *ZT* values during repeated measurements. Temperature dependence of (d) power factor (*PF*), (e) thermal conductivity (κ), and (f) *ZT* values

of different batches.

The thermoelectric conversion efficiency for a p-type $(AgCu)_{0.995}Te_{0.9}Se_{0.1}$-based single leg as a function of the hot-side temperature (T_h) was measured with a home-made system (Fig. 5). The experimental values of output power (P), thermal conductivity (κ), and conversion efficiency (η) were calculated from Fig. S17 (Supporting Information). The theoretical values of output power, thermal conductivity, and conversion efficiency were calculated based on the data of $(AgCu)_{0.995}Te_{0.9}Se_{0.1}$ given in Fig. 3(a)-(c), in which electrical and thermal contact resistances, increasing cold-side temperature during the measurement, and other heat losses are not considered.

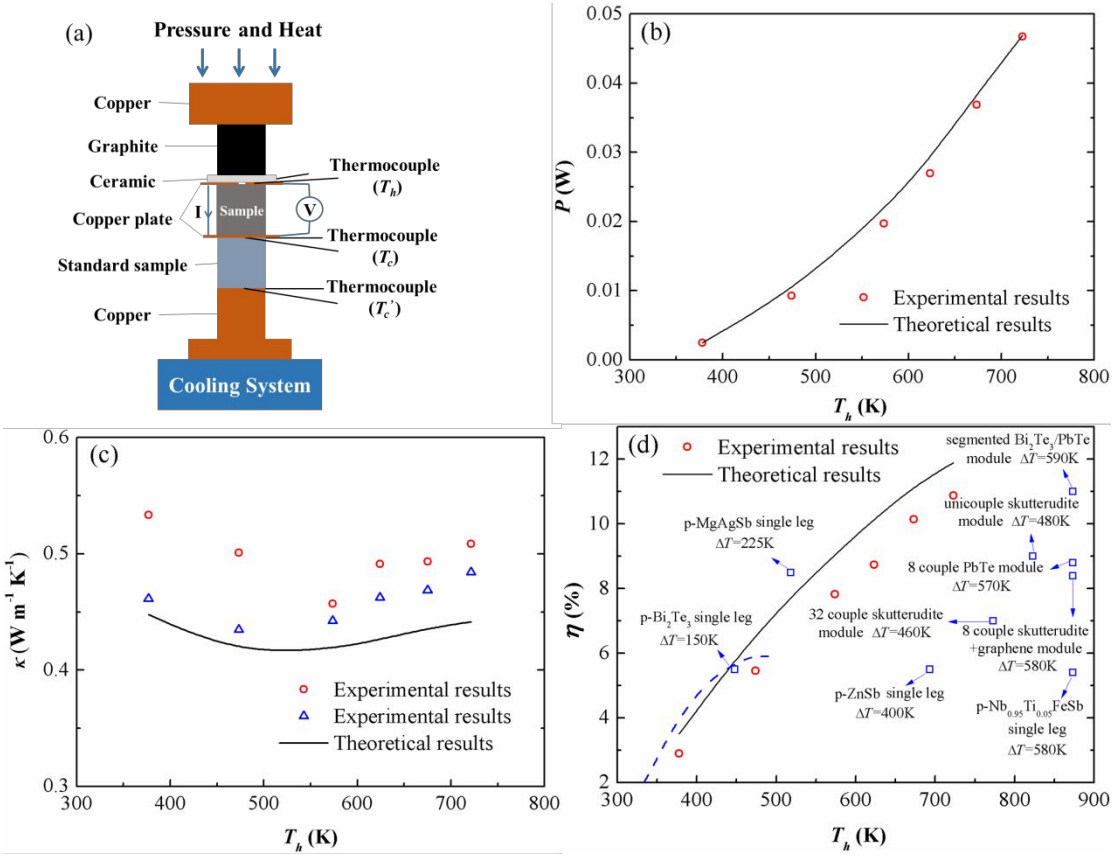

Fig. 5. Thermoelectric conversion efficiency for a p-type $(AgCu)_{0.995}Te_{0.9}Se_{0.1}$ single leg. (a) Schematic diagram of the measurement setup. (b) Experimental and theoretical output power (P) as a function of the hot-side temperature (T_h). (c) Experimental and theoretical thermal conductivity (κ) as a function of T_h using different standard samples: Constantane (red circles) or Mg_3Sb_2 (blue triangles). (d) Experimental and theoretical conversion efficiency (η) as a function of T_h. The reported maximum efficiencies of other materials are shown for comparison (p-type single legs: Bi_2Te_3 [44, 70], MgAgSb [44, 70], $Nb_{0.95}Ti_{0.05}FeSb$ [71], and ZnSb [72]; modules: unicouple skutterudite module [73], 8-couple skutterudite+graphene module [74], 32-couple skutterudite module [75], 8-couple PbTe module [76], and segmented Bi_2Te_3/PbTe module [76]).

The experimental and calculated output powers agree very well with each other [Fig. 5(b)], indicating the negligible contact resistance in this single-leg device, and confirming the reliability of the electrical conductivity and Seebeck coefficient measurements. When using Constantane as a standard sample, the experimental thermal conductivity is much higher than the theoretical value [red circles in Fig. 5(c)]. This is because the thermal conductivity of Constantane is much larger than that of the sample, which leads to a large experimental error due to the small temperature difference across the Constantane, as discussed in the Supporting Information. By changing the standard sample to Mg_3Sb_2 with closer thermal conductivities (1-1.05 W m^{-1} K^{-1} at 300-400 K [77]) to those of $(AgCu)_{0.995}Te_{0.9}Se_{0.1}$ (0.4-0.45 W m^{-1} K^{-1} at 300-400 K), the error becomes smaller and the experimental results show good agreement with the theoretical values [blue triangles in Fig. 5(c)]. Such agreement indicates the isotropic property of the $(AgCu)_{0.995}Te_{0.9}Se_{0.1}$ sample since the experimental and theoretical values of the thermal conductivity are obtained in two directions perpendicular and parallel to the pressing direction, respectively.

Due to the heat losses by radiation, the temperature rising of the cold side during the measurement, and the thermal contact resistance, the experimental efficiency values are lower than the theoretical values [Fig. 5(d)]. With the hot-/cold-side temperatures of 473 K/304 K and current density of 2.8 A cm^{-2}, the $(AgCu)_{0.995}Te_{0.9}Se_{0.1}$-based single leg yields an efficiency of 5.5%, comparable to that of the p-type Bi_2Te_3-based single leg with a similar temperature difference (ΔT) [44, 70], and similar to that of the state-of-the-art p-type single-leg devices with much larger ΔT [71, 72]. The efficiency increases almost linearly with T_h. Due to the high low-temperature performance and enhanced average ZT, the efficiency of about 11% with hot-/cold-side temperatures of 723 K/322 K and current density of 6.8 A cm^{-2} was obtained, which is higher than the previously reported maximum efficiency of other state-of-the-art materials even when they are under a much larger ΔT [Fig. 5(d)] [73-76]. The high efficiency is comparable to that of Bi_2Te_3/PbTe segmented legs with almost 1.5 times of the ΔT [76] [Fig. 5(d)]. The much lower operating

temperature of $(AgCu)_{0.995}Te_{0.9}Se_{0.1}$, combined with its high efficiency, will greatly promote its application in power generation for low- and medium-grade waste heat.

Conclusions

In summary, we have achieved a highly enhanced room-temperature power factor and strongly suppressed thermal conductivity in copper chalcogenide $(AgCu)_{0.995}Te_{0.9}Se_{0.1}$ by realizing the FCC phase at room temperature. As a result, a maximum *ZT* of ~1.1 at 350 K and an average *ZT* of ~1.0 between 300 K and 673 K have been obtained. The elevated performance is confirmed by the high conversion efficiency of 11% measured by a $(AgCu)_{0.995}Te_{0.9}Se_{0.1}$–based single-leg device. Moreover, the excellent stability and reproducibility of this material make it a promising candidate for applications. Importantly, in future studies, it is likely that the room-temperature performance of $(AgCu)_{1-x}Te_{1-z}Se_z$ will be further improved by reducing the impurities. We expect that this high-performance copper chalcogenide could be a promising complement for Bi_2Te_3, and that it will attract more attention to this material family for potential applications in waste-heat power generation and, even more importantly, for portable cooling systems.

Methods

Silver (Ag, Atlantic Metals & Alloys LLC, 99.99%, grains), copper (Cu, Alfa Aesar, 99.5%, grains), tellurium (Te, Alfa Aesar, 99.9%, chunks), and selenium (Se, Alfa Aesar, 99.9%, grains) were weighed according to the stoichiometry of $(Ag_yCu_{2-y})_{1-x}Te_{1-z}Se_z$, where the variance of x from -0.025 to 0.075 is used for optimization of the electrical conductivity, and that of y and z from 0.6 to 1.4 and from 0 to 0.25, respectively, are used for optimization of the room-temperature phase relation. All of the elements were loaded into a stainless-steel jar with stainless-steel balls and then sealed in an argon atmosphere inside a glove box for mechanical alloying by a high-energy ball mill (SPEX 8000D) for 15 h. The resulting nanopowders of about 2 g (4.5 g for efficiency measurements) were loaded into a graphite die with an inner hole diameter of 12.7 mm and then hot-pressed at 473 K

under 77 MPa for 5 min with a heating rate of 100 K min^{-1}. The hot-pressed sample was cooled down naturally in the air.

Room-temperature X-ray diffraction (XRD) spectra were collected using a PANalytical multipurpose diffractometer with an X'celerator detector (PANalytical X'Pert Pro). Temperature-dependent XRD spectra were collected using a DX-2700B (HAOYUAN China). The TEM and EDS analyses were conducted using a FEI Tecnai G2 F30 300KV. The SEM analysis and EDS mapping were conducted using a Zeiss Gemini LEO 1525 FEG, a JEOL JSM-6330F, and a JEOL JSM-7800F. The electrical conductivity (σ) and Seebeck coefficient (S) were simultaneously measured on a commercial system (ZEM-3, ULVAC) using the four-point direct-current switching method and the static temperature difference method. The total thermal conductivity (κ) was calculated using the equation $\kappa = D\rho_D Cp$, where thermal diffusivity (D) was measured using a laser flash apparatus (LFA 457, NETZSCH), volumetric density (ρ_D) was measured by the Archimedes method, and specific heat (Cp) was calculated from the Dulong–Petit law. Lattice thermal conductivity (κ_L) was calculated from $\kappa_L = \kappa - \kappa_e$, in which κ_e is defined as $\kappa_e = L_0 \sigma T$, where L_0 is the Lorenz number with an estimated value of ~1.6×10^{-8}-1.8×10^{-8} $V^2 K^{-2}$ based on the single band model and electron-phonon interactions. Considering the uncertainties from all thermoelectric parameters, the measurement of electrical conductivity σ, Seebeck coefficient S, and total thermal conductivity κ (from the thermal diffusivity D, volumetric density ρ_D, and specific heat Cp), the uncertainty for final ZT is about 20% [78]. The Hall carrier concentration (p_H) at room temperature was calculated by $p_H = 1/(eR_H)$, where Hall coefficient (R_H) was measured by a Physical Properties Measurement System (PPMS D060, Quantum Design). The output power (P) and conversion efficiency (η) were measured using a home-made apparatus. A detailed description of the measurement setup is provided in the Supporting Information and in Ref [71, 79].

Acknowledgments

The work performed at the University of Houston is supported by the U.S. Department of Energy, Office of Basic Energy Sciences, under Award Number DE-SC0010831. J. Jiang and C. Wang acknowledge the China Scholarship Council (No. 201706075009), the National Natural Science Foundation of China (Nos. 61604031, 61727818, and 51672037), and the Department of Science and Technology of Sichuan Province (No. 2019YFH0009).

Author contributions

J. Jiang prepared the samples and measured the thermoelectric properties. H. Zhu performed the characterization and analysis of structural properties. Q. Zhu and S. Song performed the conversion efficiency measurements and analysis. J. Jiang, H. Zhu, C. Wang, and Z. Ren wrote and edited the manuscript. All the authors shared ideas and contributed to the interpretation of the results.

References

[1] L. E. Bell, "Cooling, heating, generating power, and recovering waste heat with thermoelectric systems," *Science,* vol. 321, pp. 1457-1461, 2008.

[2] Y. Pei, X. Shi, A. LaLonde, H. Wang, L. Chen, and G. J. Snyder, "Convergence of electronic bands for high performance bulk thermoelectrics," *Nature,* vol. 473, pp. 66, 2011.

[3] Q. Zhang, F. Cao, W. Liu, K. Lukas, B. Yu, S. Chen*, et al.*, "Heavy doping and band engineering by potassium to improve the thermoelectric figure of merit in p-type PbTe, PbSe, and $PbTe_{1-y}Se_y$," *Journal of the American chemical society,* vol. 134, pp. 10031-10038, 2012.

[4] C. Fu, T. Zhu, Y. Liu, H. Xie, and X. Zhao, "Band engineering of high performance p-type FeNbSb based half-Heusler thermoelectric materials for figure of merit zT> 1," *Energy & Environmental Science,* vol. 8, pp. 216-220, 2015.

[5] X. Tan, H. Wang, G. Liu, J. G. Noudem, H. Hu, J. Xu*, et al.*, "Designing band engineering for thermoelectrics starting from the periodic table of elements," *Materials Today Physics,* vol. 7, pp. 35-44, 2018.

[6] L.-D. Zhao, S.-H. Lo, J. He, H. Li, K. Biswas, J. Androulakis*, et al.*, "High performance thermoelectrics from earth-abundant materials: enhanced figure of merit in PbS by second phase nanostructures," *Journal of the American Chemical Society,* vol. 133, pp. 20476-20487, 2011.

[7] S. Johnsen, J. He, J. Androulakis, V. P. Dravid, I. Todorov, D. Y. Chung*, et al.*, "Nanostructures boost the thermoelectric performance of PbS," *Journal of the American Chemical Society,* vol. 133, pp. 3460-3470, 2011.

[8] W. Kim, J. Zide, A. Gossard, D. Klenov, S. Stemmer, A. Shakouri*, et al.*, "Thermal

conductivity reduction and thermoelectric figure of merit increase by embedding nanoparticles in crystalline semiconductors," *Physical Review Letters,* vol. 96, pp. 045901, 2006.

[9] J. He, J. R. Sootsman, S. N. Girard, J.-C. Zheng, J. Wen, Y. Zhu*, et al.*, "On the origin of increased phonon scattering in nanostructured PbTe based thermoelectric materials," *Journal of the American Chemical Society,* vol. 132, pp. 8669-8675, 2010.

[10] S. H. Lo, J. He, K. Biswas, M. G. Kanatzidis, and V. P. Dravid, "Phonon Scattering and Thermal Conductivity in p-Type Nanostructured PbTe-BaTe Bulk Thermoelectric Materials," *Advanced Functional Materials,* vol. 22, pp. 5175-5184, 2012.

[11] C. Fu, H. Wu, Y. Liu, J. He, X. Zhao, and T. Zhu, "Enhancing the Figure of Merit of Heavy-Band Thermoelectric Materials Through Hierarchical Phonon Scattering," *Advanced Science,* vol. 3, pp. 1600035, 2016.

[12] B. Poudel, Q. Hao, Y. Ma, and Y. Lan, "High-thermoelectric performance of nanostructured bismuth antimony telluride bulk alloys," *Science,* vol. 320, pp. 634, 2008.

[13] J. P. Heremans, V. Jovovic, E. S. Toberer, A. Saramat, K. Kurosaki, A. Charoenphakdee*, et al.*, "Enhancement of Thermoelectric Efficiency in PbTe by Distortion of the Electronic Density of States," *Science,* vol. 321, pp. 554-557, 2008.

[14] J. P. Heremans, B. Wiendlocha, and A. M. Chamoire, "Resonant levels in bulk thermoelectric semiconductors," *Energy & Environmental Science,* vol. 5, pp. 5510-5530, 2012.

[15] Q. Zhang, H. Wang, W. Liu, H. Wang, B. Yu, Q. Zhang*, et al.*, "Enhancement of thermoelectric figure-of-merit by resonant states of aluminium doping in lead selenide," *Energy & Environmental Science,* vol. 5, pp. 5246-5251, 2012.

[16] Q. Zhang, B. Liao, Y. Lan, K. Lukas, W. Liu, K. Esfarjani*, et al.*, "High thermoelectric performance by resonant dopant indium in nanostructured SnTe," *Proceedings of the National Academy of Sciences,* vol. 110, pp. 13261-6, 2013.

[17] G. Tan, F. Shi, S. Hao, H. Chi, L. D. Zhao, C. Uher*, et al.*, "Codoping in SnTe: Enhancement of Thermoelectric Performance through Synergy of Resonance Levels and Band Convergence," *Journal of the American Chemical Society,* vol. 137, pp. 5100-12, 2015.

[18] G. Tan, W. G. Zeier, F. Shi, P. Wang, G. J. Snyder, V. P. Dravid*, et al.*, "High Thermoelectric Performance SnTe–In_2Te_3 Solid Solutions Enabled by Resonant Levels and Strong Vacancy Phonon Scattering," *Chemistry of Materials,* vol. 27, pp. 7801-7811, 2015.

[19] K. Biswas, J. He, I. D. Blum, C.-I. Wu, T. P. Hogan, D. N. Seidman*, et al.*, "High-performance bulk thermoelectrics with all-scale hierarchical architectures," *Nature,* vol. 489, pp. 414, 2012.

[20] J. Shuai, J. Mao, S. Song, Q. Zhang, G. Chen, and Z. Ren, "Recent progress and future challenges on thermoelectric Zintl materials," *Materials Today Physics,* vol. 1, pp. 74-95, 2017.

[21] J. Shuai, J. Mao, S. Song, Q. Zhu, J. Sun, Y. Wang*, et al.*, "Tuning the carrier scattering mechanism to effectively improve the thermoelectric properties," *Energy & Environmental Science,* vol. 10, pp. 799-807, 2017.

[22] J. Mao, J. Shuai, S. Song, Y. Wu, R. Dally, J. Zhou*, et al.*, "Manipulation of ionized impurity scattering for achieving high thermoelectric performance in n-type Mg_3Sb_2-based materials," *Proceedings of the National Academy of Sciences,* pp. 201711725, 2017.

[23] S. Ohno, U. Aydemir, M. Amsler, J.-H. Pöhls, S. Chanakian, A. Zevalkink*, et al.*, "Achieving $zT > 1$ in Inexpensive Zintl Phase $Ca_9Zn_{4+x}Sb_9$ by Phase Boundary Mapping," *Advanced*

Functional Materials, vol. 27, pp. 1606361, 2017.

[24] K. F. Hsu, S. Loo, F. Guo, W. Chen, J. S. Dyck, C. Uher*, et al.*, "Cubic $AgPb_mSbTe_{2+m}$: Bulk thermoelectric materials with high figure of merit," *Science,* vol. 303, pp. 818-821, 2004.

[25] B. Sales, D. Mandrus, and R. K. Williams, "Filled skutterudite antimonides: a new class of thermoelectric materials," *Science,* vol. 272, pp. 1325-1328, 1996.

[26] X. Meng, Z. Liu, B. Cui, D. Qin, H. Geng, W. Cai*, et al.*, "Grain Boundary Engineering for Achieving High Thermoelectric Performance in n-Type Skutterudites," *Advanced Energy Materials,* vol. 7, pp. 1602582, 2017.

[27] X. Shi, J. Yang, J. R. Salvador, M. Chi, J. Y. Cho, H. Wang*, et al.*, "Multiple-filled skutterudites: high thermoelectric figure of merit through separately optimizing electrical and thermal transports," *Journal of the American Chemical Society,* vol. 133, pp. 7837-7846, 2011.

[28] Y. Liu, L. M. Wu, L. H. Li, S. W. Du, J. D. Corbett, and L. Chen, "The Antimony-Based Type I Clathrate Compounds $Cs_8Cd_{18}Sb_{28}$ and $Cs_8Zn_{18}Sb_{28}$," *Angewandte Chemie International Edition,* vol. 121, pp. 5409-5412, 2009.

[29] T. Takabatake, K. Suekuni, T. Nakayama, and E. Kaneshita, "Phonon-glass electron-crystal thermoelectric clathrates: Experiments and theory," *Reviews of Modern Physics,* vol. 86, pp. 669, 2014.

[30] L.-D. Zhao, S.-H. Lo, Y. Zhang, H. Sun, G. Tan, C. Uher*, et al.*, "Ultralow thermal conductivity and high thermoelectric figure of merit in SnSe crystals," *Nature,* vol. 508, pp. 373-377, 2014.

[31] H. Liu, X. Shi, F. Xu, L. Zhang, W. Zhang, L. Chen*, et al.*, "Copper ion liquid-like thermoelectrics," *Nature Materials,* vol. 11, pp. 422-5, 2012.

[32] Y. He, T. Day, T. Zhang, H. Liu, X. Shi, L. Chen*, et al.*, "High thermoelectric performance in non-toxic earth-abundant copper sulfide," *Advanced Materials,* vol. 26, pp. 3974-8, 2014.

[33] Y. He, P. Lu, X. Shi, F. Xu, T. Zhang, G. J. Snyder*, et al.*, "Ultrahigh Thermoelectric Performance in Mosaic Crystals," *Advanced Materials,* vol. 27, pp. 3639-44, 2015.

[34] S. Roychowdhury, M. K. Jana, J. Pan, S. N. Guin, D. Sanyal, U. V. Waghmare*, et al.*, "Soft Phonon Modes Leading to Ultralow Thermal Conductivity and High Thermoelectric Performance in AgCuTe," *Angewandte Chemie International Edition,* vol. 57, pp. 4043-4047, 2018.

[35] S. D. Kang, J.-H. Pöhls, U. Aydemir, P. Qiu, C. C. Stoumpos, R. Hanus*, et al.*, "Enhanced stability and thermoelectric figure-of-merit in copper selenide by lithium doping," *Materials Today Physics,* vol. 1, pp. 7-13, 2017.

[36] T. W. Day, W. G. Zeier, D. R. Brown, B. C. Melot, and G. J. Snyder, "Determining conductivity and mobility values of individual components in multiphase composite $Cu_{1.97}Ag_{0.03}Se$," *Applied Physics Letters*, vol. 105, pp. 172103, 2014.

[37] S. Ahmad, A. Singh, A. Bohra, R. Basu, S. Bhattacharya, R. Bhatt*, et al.*, "Boosting thermoelectric performance of p-type SiGe alloys through in-situ metallic YSi_2 nanoinclusions," *Nano Energy,* vol. 27, pp. 282-297, 2016.

[38] K. Xia, Y. Liu, S. Anand, G. J. Snyder, J. Xin, J. Yu*, et al.*, "Enhanced Thermoelectric Performance in 18-Electron $Nb_{0.8}CoSb$ Half-Heusler Compound with Intrinsic Nb Vacancies," *Advanced Functional Materials,* vol. 28, pp. 1705845, 2018.

[39] W. Ren, H. Zhu, Q. Zhu, U. Saparamadu, R. He, Z. Liu*, et al.*, "Ultrahigh Power Factor in

Thermoelectric System $Nb_{0.95}M_{0.05}FeSb$ (M= Hf, Zr, and Ti)," *Advanced Science,* pp. 1800278, 2018.

[40] C. Hu, K. Xia, X. Chen, X. Zhao, and T. Zhu, "Transport mechanisms and property optimization of p-type (Zr, Hf)CoSb half-Heusler thermoelectric materials," *Materials Today Physics,* vol. 7, pp. 69-76, 2018.

[41] Y. Liu, Y. Zhang, K. H. Lim, M. Ibáñez, S. Ortega, M. Li, J. David, S. M.-Sánchez, K. M. Ng, J. Arbiol, M. V. Kovalenko, D. Cadavid, and A. Cabot, "High Thermoelectric Performance in Crystallographically Textured n-Type $Bi_2Te_{3-x}Se_x$ Produced from Asymmetric Colloidal Nanocrystals," *ACS Nano*, vol. 12, pp. 7174–7184, 2018.

[42] Y. Liu, Y. Zhang, S. Ortega, M. Ibáñez, K. H. Lim, A. G.-Carbonell, S. M.-Sánchez, K. M. Ng, J. Arbiol, M. V. Kovalenko, D. Cadavid, and A. Cabot, "Crystallographically Textured Nanomaterials Produced from the Liquid Phase Sintering of $Bi_xSb_{2-x}Te_3$ Nanocrystal Building Blocks," Nano Letters, vol. 18, pp. 2557–2563, 2018.

[43] H. J. Goldsmid, "Bismuth telluride and its alloys as materials for thermoelectric generation," *Materials,* vol. 7, pp. 2577-2592, 2014.

[44] D. Kraemer, J. Sui, K. McEnaney, H. Zhao, Q. Jie, Z. F. Ren*, et al.*, "High thermoelectric conversion efficiency of MgAgSb-based material with hot-pressed contacts," *Energy & Environmental Science,* vol. 8, pp. 1299-1308, 2015.

[45] Z. Liu, Y. Wang, J. Mao, H. Geng, J. Shuai, Y. Wang*, et al.*, "Lithium doping to enhance thermoelectric performance of MgAgSb with weak electron–phonon coupling," *Advanced Energy Materials,* vol. 6, pp. 1502269, 2016.

[46] W. Li, S. Lin, B. Ge, J. Yang, W. Zhang, and Y. Pei, "Low sound velocity contributing to the high thermoelectric performance of Ag_8SnSe_6," *Advanced Science,* vol. 3, pp. 1600196, 2016.

[47] Z.-H. Ge, D. Song, X. Chong, F. Zheng, L. Jin, X. Qian*, et al.*, "Boosting the Thermoelectric Performance of (Na, K)-Codoped Polycrystalline SnSe by Synergistic Tailoring of the Band Structure and Atomic-Scale Defect Phonon Scattering," *Journal of the American Chemical Society,* vol. 139, pp. 9714-9720, 2017.

[48] J.-Y. Tak, W. H. Nam, C. Lee, S. Kim, Y. S. Lim, K. Ko*, et al.*, "Ultralow Lattice Thermal Conductivity and Significantly Enhanced Near-Room-Temperature Thermoelectric Figure of Merit in α-Cu_2Se through Suppressed Cu Vacancy Formation by Overstoichiometric Cu Addition," *Chemistry of Materials,* vol. 30, pp. 3276-3284, 2018.

[49] Y. Sun, L. Xi, J. Yang, L. Wu, X. Shi, L. Chen*, et al.*, "The "electron crystal" behavior in copper chalcogenides Cu_2X (X = Se, S)," *Journal of Materials Chemistry A,* vol. 5, pp. 5098-5105, 2017.

[50] H. Chen, H. Lin, Z. X. Lin, J. N. Shen, L. Chen, and L. M. Wu, "Superionic adjustment leading to weakly temperature-dependent ZT values in bulk thermoelectrics," *Inorg Chem,* vol. 54, pp. 867-71, 2015.

[51] A. J. Hong, L. Li, H. X. Zhu, X. H. Zhou, Q. Y. He, W. S. Liu*, et al.*, "Anomalous transport and thermoelectric performances of CuAgSe compounds," *Solid State Ionics,* vol. 261, pp. 21-25, 2014.

[52] P. Qiu, X. Shi, and L. Chen, "Cu-based thermoelectric materials," *Energy Storage Materials,* vol. 3, pp. 85-97, 2016.

[53] N. Vouroutzis, N. Frangis, and C. Manolikas, "The double modulation superstructure of the room temperature stable phase of stoichiometric Cu_2Te," *Physica Status Solidi (a),* vol. 202,

pp. 271-280, 2005.

[54] Y. G. Asadov, Y. I. Aliyev, and A. G. Babaev, "Polymorphic transformations in Cu_2Se, Ag_2Se, AgCuSe and the role of partial cation-cation and anion-anion replacement in stabilizing their modifications," *Physics of Particles and Nuclei,* vol. 46, pp. 452-474, 2015.

[55] M. C. Nguyen, J.-H. Choi, X. Zhao, C.-Z. Wang, Z. Zhang, and K.-M. Ho, "New layered structures of cuprous chalcogenides as thin film solar cell materials: Cu_2Te and Cu_2Se," *Physical Review Letters,* vol. 111, pp. 165502, 2013.

[56] P. Lu, H. Liu, X. Yuan, F. Xu, X. Shi, K. Zhao*, et al.*, "Multiformity and fluctuation of Cu ordering in Cu_2Se thermoelectric materials," *Journal of Materials Chemistry A,* vol. 3, pp. 6901-6908, 2015.

[57] Y. He, T. Zhang, X. Shi, S.-H. Wei, and L. Chen, "High thermoelectric performance in copper telluride," *NPG Asia Materials,* vol. 7, pp. e210-e210, 2015.

[58] T. Mao, P. Qiu, P. Hu, X. Du, K. Zhao, T.-R. Wei, *et al.*, "Decoupling Thermoelectric Performance and Stability in Liquid-Like Thermoelectric Materials," *Advanced Science,* pp. 1901598, 2019.

[59] K. Zhao, K. Liu, Z. Yue, Y. Wang, Q. Song, J. Li, *et al.*, "Are Cu_2Te-Based Compounds Excellent Thermoelectric Materials?" *Advanced Materials,* pp. 1903480, 2019.

[60] D. Zhang, J. Yang, H. Bai, Y. Luo, B. Wang, S. Hou, *et al.*, "Significant average *ZT* enhancement in Cu_3SbSe_4-based thermoelectric material via softening p–d hybridization," *Journal of Materials Chemistry A,* DOI: 10.1039/c9ta05115e, 2019.

[61] T. J. Slade, T. P. Bailey, J. A. Grovogui, X. Hua, X. Zhang, J. J. Kuo, *et al.*, "High Thermoelectric Performance in PbSe–$NaSbSe_2$ Alloys from Valence Band Convergence and Low Thermal Conductivity," *Advanced Energy Materials,* pp. 1901377, 2019.

[62] Y. Xing, R. Liu, J. Liao, Q. Zhang, X. Xia, C. Wang, *et al.*, "High-efficiency half-Heusler thermoelectric modules enabled by self-propagating synthesis and topologic structure optimization," *Energy & Environmental Science,* vol. 12, pp. 3390-3399, 2019.

[63] Z. Liu, S. Guo, Y. Wu, J. Mao, Q. Zhu, H. Zhu, *et al.*, " Design of High-Performance Disordered Half-Heusler Thermoelectric Materials Using 18-Electron Rule," *Advanced Functional Materials,* vol. 29, pp. 1905044, 2019.

[64] H. S. Kim, W. Liu, G. Chen, C. W. Chu, and Z. Ren, "Relationship between thermoelectric figure of merit and energy conversion efficiency," *Proceedings of the National Academy of Sciences,* vol. 112, pp. 8205-10, 2015.

[65] J. Li, X. Zhang, Z. Chen, S. Lin, W. Li, J. Shen*, et al.*, "Low-symmetry rhombohedral GeTe thermoelectrics," *Joule,* vol. 2, pp. 976-987, 2018.

[66] W. Zhao, Z. Liu, Z. Sun, Q. Zhang, P. Wei, X. Mu*, et al.*, "Superparamagnetic enhancement of thermoelectric performance," *Nature,* vol. 549, pp. 247, 2017.

[67] G. Joshi, X. Yan, H. Wang, W. Liu, G. Chen, and Z. Ren, "Enhancement in thermoelectric figure-of-merit of an N-type half-Heusler compound by the nanocomposite approach," *Advanced Energy Materials,* vol. 1, pp. 643-647, 2011.

[68] L. Yang, Z.-G. Chen, M. S. Dargusch, and J. Zou, "High Performance Thermoelectric Materials: Progress and Their Applications," *Advanced Energy Materials,* vol. 8, pp. 1701797, 2018.

[69] C. Chang and L.-D. Zhao, "Anharmoncity and low thermal conductivity in thermoelectrics," *Materials Today Physics,* vol. 4, pp. 50-57, 2018.

[70] Z. Liu, J. Mao, J. Sui, and Z. Ren, "High thermoelectric performance of α-MgAgSb for power generation," *Energy & Environmental Science,* vol. 11, pp. 23-44, 2018.

[71] R. He, D. Kraemer, J. Mao, L. Zeng, Q. Jie, Y. Lan*, et al.*, "Achieving high power factor and output power density in p-type half-Heuslers $Nb_{1-x}Ti_xFeSb$," *Proceedings of the National Academy of Sciences,* vol. 113, pp. 13576-13581, 2016.

[72] M. Telkes, "Solar Thermoelectric Generators," *Journal of Applied Physics,* vol. 25, pp. 765-777, 1954.

[73] A. Muto, J. Yang, B. Poudel, Z. Ren, and G. Chen, "Skutterudite Unicouple Characterization for Energy Harvesting Applications," *Advanced Energy Materials,* vol. 3, pp. 245-251, 2013.

[74] P.-a. Zong, R. Hanus, M. Dylla, Y. Tang, J. Liao, Q. Zhang*, et al.*, "Skutterudite with graphene-modified grain-boundary complexion enhances zT enabling high-efficiency thermoelectric device," *Energy & Environmental Science,* vol. 10, pp. 183-191, 2017.

[75] J. R. Salvador, J. Y. Cho, Z. Ye, J. E. Moczygemba, A. J. Thompson, J. W. Sharp*, et al.*, "Conversion efficiency of skutterudite-based thermoelectric modules," *Physical Chemistry Chemical Physics,* vol. 16, pp. 12510-20, 2014.

[76] X. Hu, P. Jood, M. Ohta, M. Kunii, K. Nagase, H. Nishiate*, et al.*, "Power generation from nanostructured PbTe-based thermoelectrics: comprehensive development from materials to modules," *Energy & Environmental Science,* vol. 9, pp. 517-529, 2016.

[77] S. Song, J. Mao, J. Shuai, H. Zhu, Z. Ren, U. Saparamadu*, et al.*, "Study on anisotropy of n-type Mg_3Sb_2-based thermoelectric materials," *Applied Physics Letters,* vol. 112, pp. 092103, 2018.

[78] C. Chang, M. Wu, D. He, Y. Pei, C.-F. Wu, X. Wu*, et al.*, "3D charge and 2D phonon transports leading to high out-of-plane ZT in n-type SnSe crystals," *Science,* vol. 360, pp. 778–783, 2018.

[79] Q. Zhu, S. Song, H. Zhu, and Z. Ren, "Realizing high conversion efficiency of Mg_3Sb_2-based thermoelectric materials," *Journal of Power Sources*, vol. 414, pp. 393-400, 2019.

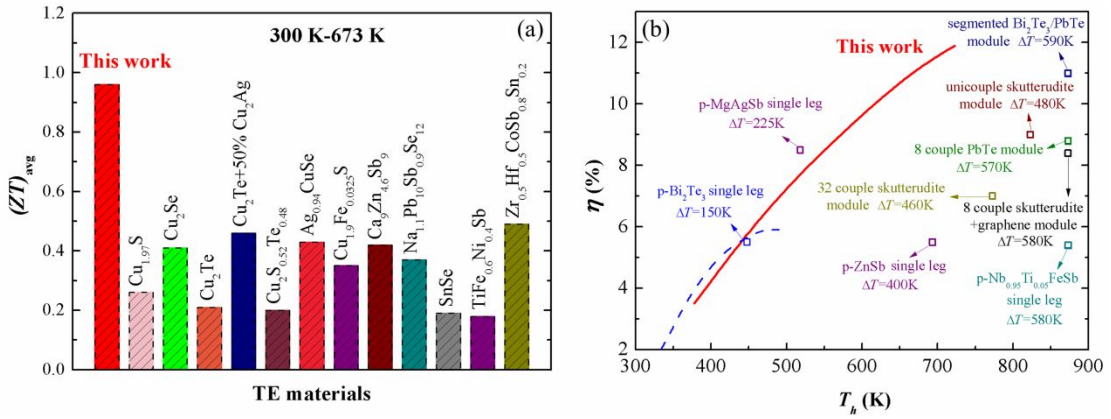

Average *ZT* of near unity provides a competitive thermoelectric conversion efficiency of ～12% at low temperature difference of 400K.